Defence Science Journal, Vol 47, No 3, July 1997, pp. 327-341

On a New Six-Degree-of-Freedom Modelling Method for Homing Missiles and its Application for Design/Analysis

R. N. Bhattacherjee and A. Saha

Defence Research & Development Laboratory, Hyderabad-500 058

ABSTRACT

Development of an accurate six-degree-of-freedom (6-DOF) simulation model for homing missiles incorporating seeker servosystem detailed modelling is reported. A new modelling concept for seeker servosystem simulation, the Newtonian equivalent model (NEM) has been evolved, where body motion coupling is modelled through forces and moments transformed to the seeker. The NEM-based modelling of seeker head and its integration in 6-DOF has been discussed. In the presence of body coupling, the simulation model for seeker tracking or pointing error, gimbal angles and inertial line of sight (LOS) rates as measured by the seeker mounted rate gyros have been obtained through the new modelling method. A novel method of obtaining optimum pitch and yaw LOS rates for proportional navigation (PN) guidance mechanisation is formulated based on synthesised sight line rates measured in the seeker inner gimbal axis. This new method has been validated through simulation studies using the 6-DOF model developed and by comparing the results with those obtained by the conventional method of generating LOS rates for PN guidance. Other important applications of the 6-DOF model discussed are guidance and control design validation/tuning, seeker feedforward compensation design, tuning of switchover point from open-loop to closed-loop PN guidance. Importance of the detailed 6-DOF simulation model as the ultimate performance evaluation tool for the weapon system, in terms of both terminal performance and adequacy of seeker field of view, gimbal angle freedom, etc. has been brought out.

NOMENCLATURE

$\dot{\omega}_b$	Angular acceleration of the base
$\dot{\omega}_1$	Angular acceleration of the motor
$\dot{\omega}_2$	Angular acceleration of the load
J_m	Motor inertia
J_L	Load inertia
ω_b^{yaw}	Yaw rate
ω_b^{pitch}	Pitch rate
ω_b^{roll}	Roll rate
ω_b^{ele}	Body rate transformed to the elevation gimbal drive system
ω_{icm}	Inertial angular rate of gimbals
ω_{bcm}	Relative gimbal rate
β, θ_g	Elevation gimbal angle
G_{couply}	Geometric coupling
α, ψ_g	Azimuth gimbal angle
n	Gear ratio of azimuth drive system
n_1	Gear ratio of elevation drive system
T_A	Motor actuation torque
T_G	Gear coupling torque
T_C	Coulomb friction torque
T_F	Friction torque
T_{ST}	Stiction torque
T_L	Azimuth gimbal torque
dh	Homing distance

Received 03 January 1997

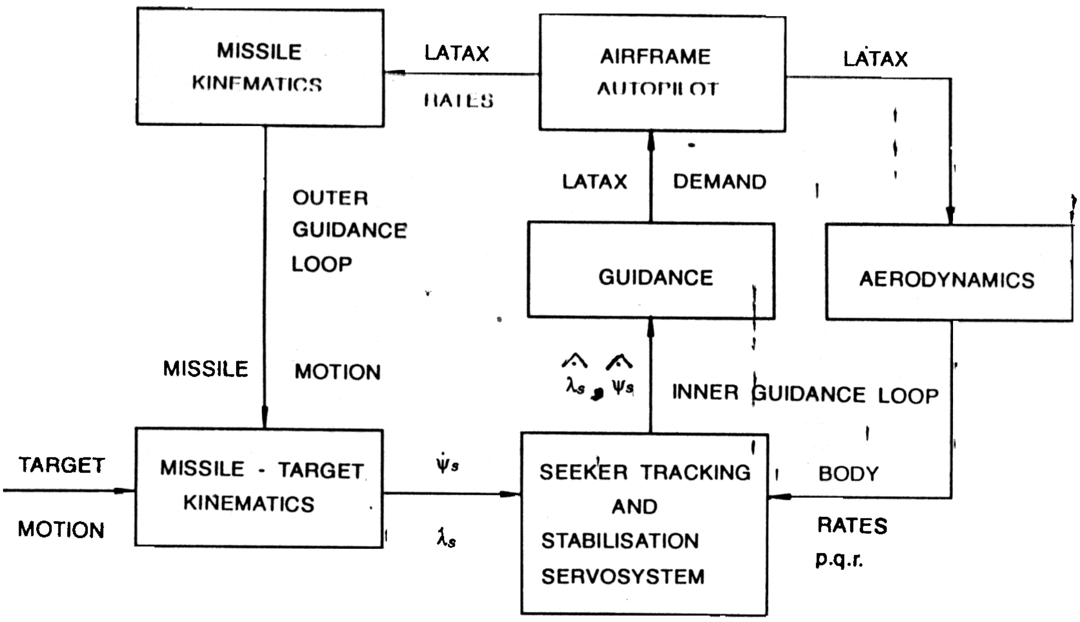

Figure 1. 6-DOF model overview

Rv_{max} Maximum relative velocity at which transition from stiction to Coulomb friction occurs

r_1 Radius of motor gear

r_2 Radius of load gear

r_{ss} Switching sight line range

HE heading error ≈ gimbal angle at switching

1. INTRODUCTION

For homing missiles, proportional navigation guidance law is normally employed, which requires line of sight (LOS) rate information from seeker-to-target. The target tracker in the missile (i.e. the seeker) is made to track the target through the tracker servosystem (outer tracking loop). In most of the homing missiles, including the system presented here, the seeker is space-stabilised in the presence of body motions with the help of a high gain inner loop (inner stabilisation loop) which uses seeker-mounted rate gyro signals for inner loop feedback. For this type of homing system, two guidance loops need to be modelled and the performance studied: (a) the outer guidance loop comprising missile-target kinematics, seeker tracking and stabilisation servosystem, guidance, airframe-autopilot combination and missile kinematics closing the loop and (b) the inner guidance loop comprising body rate to LOS rate coupling dynamics, guidance, autopilot and missile aerodynamics closing the loop.

Development of an accurate six-degree-of-freedom (6-DOF) simulation model covering the above-mentioned outer and inner guidance loops has been briefly discussed in this paper. Fig. 1 shows a brief overview of 6-DOF model, including different subsystems. The work done includes the development of a new method of modelling the body motion coupling to homing head and a novel method of obtaining optimum pitch and yaw LOS rates for proportion navigation (PN) guidance.

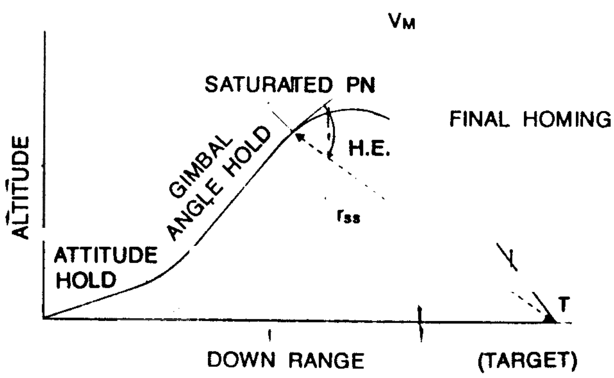

Figure 2. Phases of guided trajectory

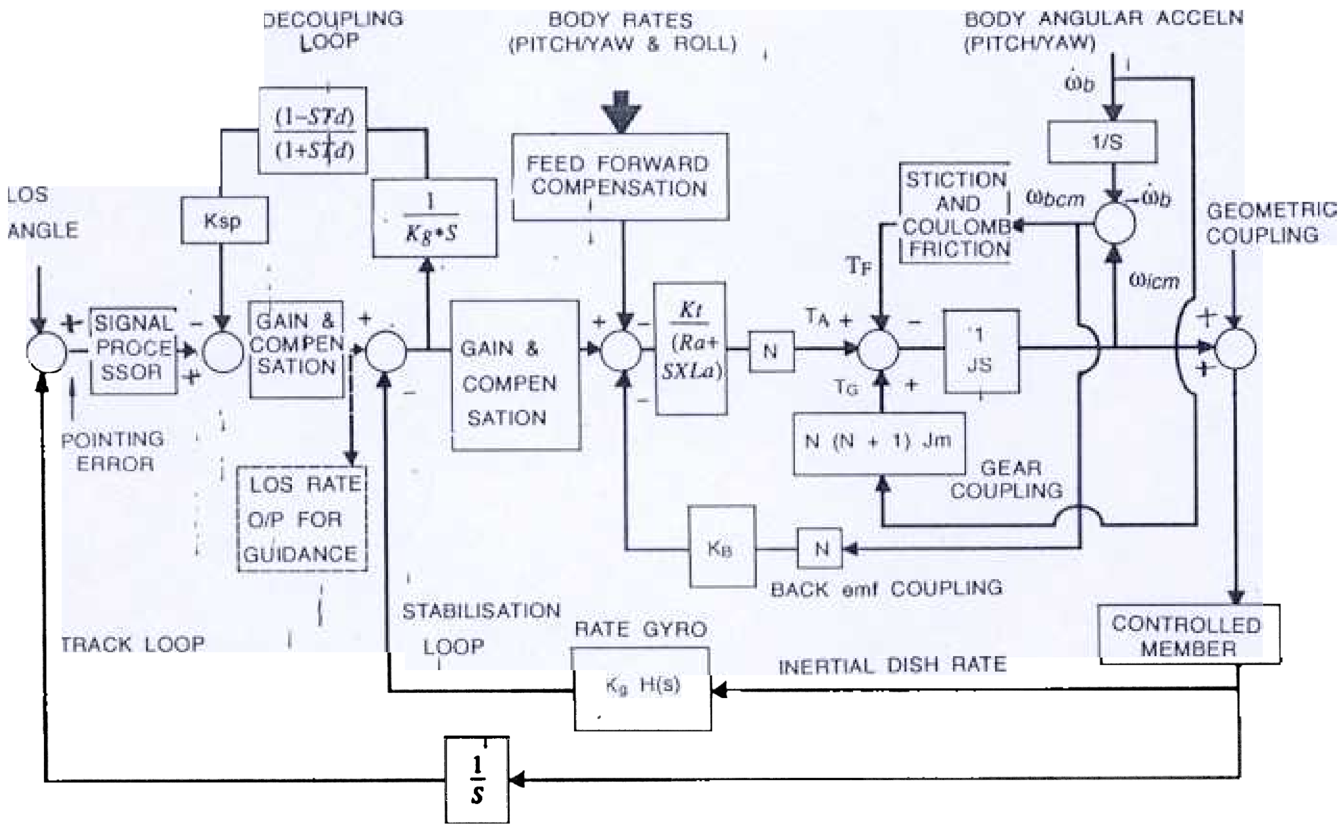

Figure 3. Seeker-servosystem model

Different possible applications of the model for design and analysis of the homing missile system have also been covered.

2. SIX-DEGREE-OF-FREEDOM MODEL

The 6-DOF simulation model consists of six equations of motion for the missile: three equations of force and three equations of moments (typical 6-DOF equations of motion are given in Appendix 1). Forces and moments affecting missile motion are mainly due to propulsion, aerodynamics and control forces/moments. The control forces/ moments are due to control deflections which have been generated based on the guidance and control algorithm. Guidance and control algorithm design has been carried out to shape the trajectory so as to meet the specified guidance accuracy and impact angle requirement.

The 6-DOF simulation model features for a third generation antitank missile (ATM) with top-attack and fire-and-forget capability is reported here. Fire-and-forget capability for ATM requires autonomous homing guidance implemented based on LOS rate obtained in this case from the imaging infrared seeker, stabilised through seeker-mounted rate gyros. However, during the initial phase, to optimise the impact angle, missile trajectory is made to pitch up as sharply as the gimbal angle limit allows through a gimbal angle hold phase in the guidance (implemented by a gimbal angle hold autopilot). The trajectory in elevation plane is depicted in Fig. 2. Switching to PN guidance is done as soon as the required sight line range or equivalently sight line rate is reached. This is done after correcting the heading error (~ gimbal angle at switching) between sight line, and flight path with minimum radius of turn capability of the configuration in the saturated PN (SPN) phase, so that enough homing distance (dh) is available for

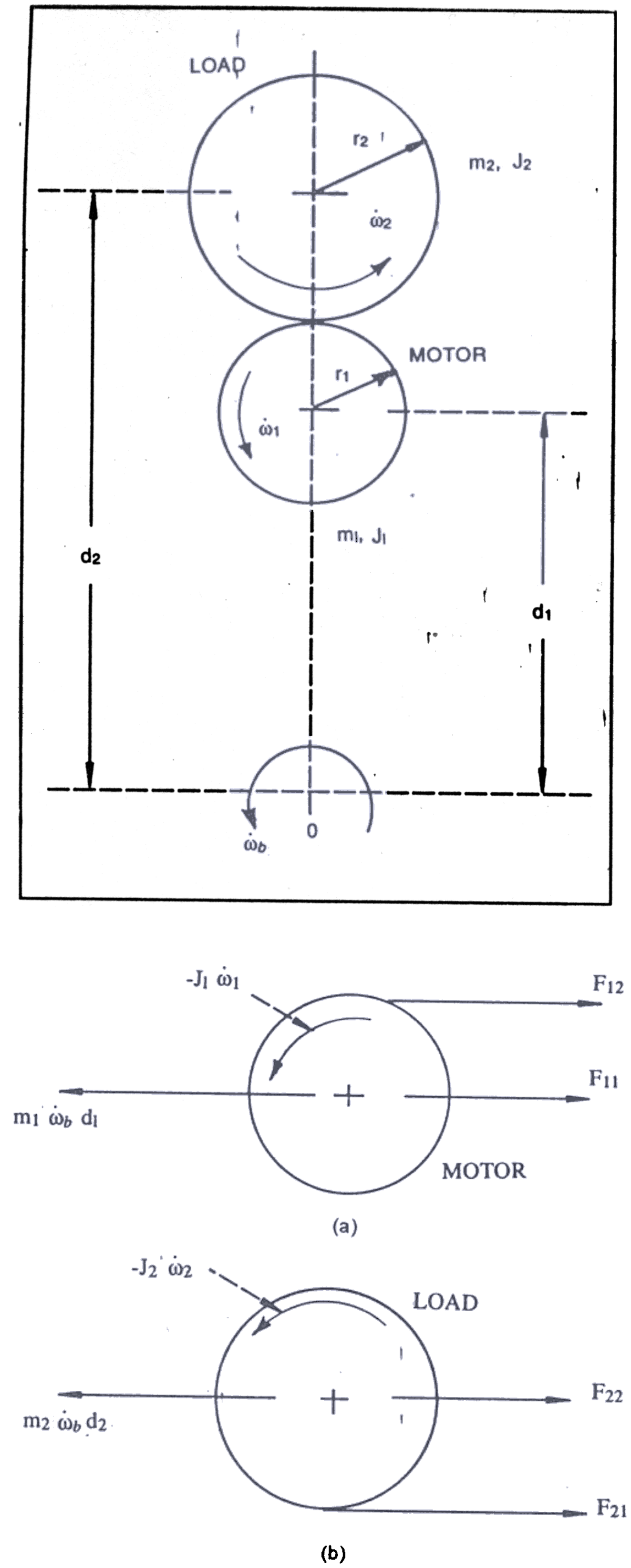

Figure 4. Base motion coupling through gears

settling the errors/transients in the final homing phase. This helps to ensure the required miss distance. Since miss distance requirement is very stringent, accurate modelling of the seeker servosystem is essential for getting the guidance parameters, i.e. gimbal angle, LOS rate, etc. very close to the actual hardware outputs for tuning guidance algorithm and predicting the miss distance accurately based on the 6-DOF model.

Seeker-servosystem model has been developed based on a new concept of body motion coupling to the seeker head, through forces and moments transformed to the seeker. This is termed as Newtonian equivalent model (NEM) and is quite different from the velocity injection model normally used, where body rate is directly injected to the seeker on 1:1 basis[1,2]. The NEM-based seeker-servosystem modelling is discussed here.

3. SEEKER-SERVOSYSTEM MODELLING

Seeker-servosystem consists of an outer track loop and an inner stabilisation loop (Fig. 3). Driving signal for the track loop is the seeker pointing error (error between LOS and seeker boresight), which it corrects by generating commanded LOS rate or disc rate signal to the inner stabilisation loop. Stabilisation loop is a high gain servosystem which stabilises the seeker with respect to body rate disturbances and follows the above commanded disc rate. In the NEM developed, the different sources of base motion coupling to the seeker are

(i) Coupling through gears (in the geared-drive system considered)

(ii) Back electromotive force (emf) coupling

(iii) Coupling through friction, and

(iv) Geometrical coupling.

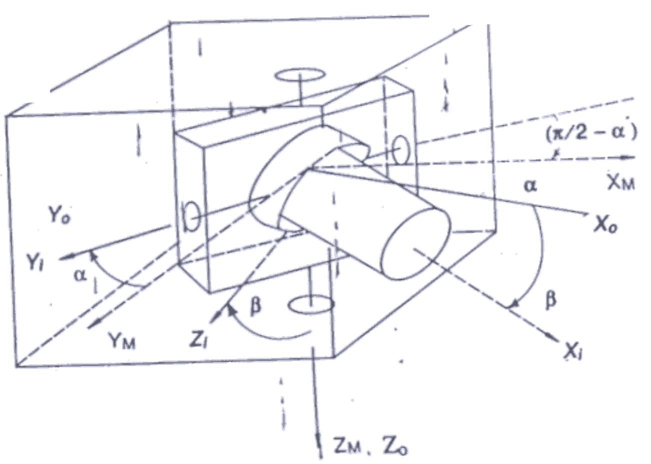

AZIMUTH GIMBAL ANGLE = α
ELEVATION GIMABL ANGLE = β

Figure 5. Seeker gimbal system

3.1 Coupling through Gears

The case of base motion coupling to the load side (i.e. seeker) due to gearing is considered in Fig. 4. $\dot{\omega}_b$, $\dot{\omega}_1$ and $\dot{\omega}_2$ are the angular acceleration of the base, the motor and the load, respectively.

The gear ratio $n = r_2/r_1$. Figures 4(a) and 4(b) give the free body diagrams for the motor and the load, respectively. F_{11} and F_{22} are bearing forces along x-axis. From the free body diagrams, the following relations are derived :

$F_{21} = -F_{12}$; at the point of mesh

also : $-J_1\dot{\omega}_1 - F_{12}r_1 = 0$

$$\text{therefore, } F_{12} = -\frac{J_1}{r_1}\dot{\omega} \tag{1}$$

again, $-J_2\dot{\omega}_2 + F_{21}r_2 = 0$

$$\text{therefore, } \dot{\omega}_2 = -F_{12}\frac{r_2}{J_2} = \frac{r_2}{r_1}\frac{J_1}{J_2}\dot{\omega}_1 \tag{2}$$

The kinematic constraint equation can be written as

$$n(\dot{\omega}_2 - \dot{\omega}_b) = -(\dot{\omega}_1 - \dot{\omega}_b) \tag{3}$$

therefore, from Eqns (2) and (3)

$$\dot{\omega}_2 = \left[\frac{n(n+1)J_1}{n^2J_1 + J_2}\right]\dot{\omega}_b \tag{4}$$

For the seeker

J_1 Motor inertia = J_m,
J_2 Load inertia = J_L, and
J Equivalent inertia referred to load side $= n^2J_1 + J_2$

Therefore, the torque transmitted to the load side ($J\dot{\omega}_2$) due to gear coupling is obtained from Eqn (4) as

$$T_L\,(\text{gear}) = n(n+1)J_m\dot{\omega}_b \tag{5}$$

For the seeker-servosystem considered, the gimbal system is shown in Fig. 5 where:
(X_M, Y_M, Z_M) - Missile body axis;

(X_o, Y_o, Z_o) - Outer gimbal axis,

(X_i, Y_i, Z_i) - Inner gimbal axis.

The azimuth gimbal rotates about body Z_M (Z_o) axis by azimuth gimbal angle α and thereafter elevation gimbal rotates about the outer gimbal Y_o (Y_i) axis by elevation gimbal angle β. Therefore, the azimuth gimbal drive will get body yaw rate only, which will contribute to azimuth gimbal torque T_L due to gear coupling as per Eqn (5) giving

$$T_L = \dot{\omega}_b^{yaw}n(n+1)J_m \tag{6}$$

For the elevation gimbal, drive motor is on the outer gimbal and rotates about the Y_o, Y_i axis. Therefore, the body pitch and roll rate (and acceleration) components along the Y_o, Y_i axis will contribute to elevation gimbal torque T_{Ll} due to gear coupling as per the equation

$$T_{Ll} = n_1(n+1)J_{m1}\dot{\omega}_b^{ele} \tag{7}$$

$$\dot{\omega}_b^{ele} = \dot{\omega}_b^{pitch}\cos\alpha \quad \dot{\omega}_b^{roll}\sin\alpha$$

3.2 Back emf Coupling

The back emf of the drive motor is obtained by transferring the relative gimbal rate ω_{bcm} to the motor side (by multiplying with gear ratio) and multiplying it by the back emf constant K_B. The relative gimbal rate is calculated by subtracting the corresponding body rate components (coupled to the gimbals) from the inertial gimbal rate in the respective planes of azimuth and elevation (Fig. 3). Due to this back emf voltage, an equivalent torque is generated, which is the back emf coupling torque.

3.3 Coupling through Friction

The friction model considers the torques generated by both static and viscous frictions. If there is no relative motion between the gimbal and the body, i.e. the relative gimbal rate ω_{bcm} is zero, then due to static friction, the gimbal will move along with the body, i.e. the body rate component on the base will be totally coupled to the load. This phenomenon is modelled as

When

$$\omega_{bcm} = 0 \;;$$

Effective torque $T_E = J\dot{\omega}_b$

By referring to Fig. 3, the corresponding friction torque is obtained as

Effective torque $T_E = J\dot{\omega}_b$ = motor torque + gear coupling torque − frictional torque

$$T_A + n(n+1)J_m\dot{\omega}_b - [T_A - X\dot{\omega}_b]$$

$$\therefore\ X = [J - n\,(n+1)\,J_m] \tag{8}$$

Therefore, with $T_A - X\dot{\omega}_b$ (X as above) modelled as friction torque (Fig. 3), the effective load torque T_E becomes equal to the body motion torque $J\dot{\omega}_b$ due to static friction, when $\omega_{bcm} = 0$.

When, there is a relative rate present between the missile body and the gimbal (i.e. $\omega_{bcm} \neq 0$), the friction torques will be generated due to stiction (for $\omega_{bcm} \leq Rv_{max}$) and due to Coulomb friction (for $\omega_{bcm} > Rv_{max}$), where Rv_{max} = Maximum relative velocity, at which the transition from stiction to Coulomb friction occurs.

Therefore, the friction model is summarised as

When

$$\omega_{bcm} = 0,$$

then

$$T_F = T_R = T_A \quad [J - n(n+1)J_m]\dot{\omega}_b$$

When

$$\omega_{bcm} \neq 0,$$

then

for $\omega_{bcm} \leq Rv_{max}$, $T_F = T_{ST}$ = Stiction torque,

and for $\omega_{bcm} > Rv_{max}$, $T_F = T_C$ = Coulomb friction torque.

3.4 Geometric Coupling

As the azimuth gimbal rotates wrt the body $Z_b \equiv$ Azimuth gimbal Z_o axis; therefore, no component of roll and pitch torques will get coupled to the azimuth gimbal drive base. However, as the azimuth rate gyro placed on the inner gimbal senses the azimuth rate wrt the inner gimbal Z_i axis, the components of body roll and pitch rates coupled to the inner gimbal Z_i axis will be sensed by the azimuth gyro. By referring to Fig. 5, this geometric coupling term in azimuth plane is obtained as

$$G_{couply} = \omega_{ib}^{roll}\cos\alpha.\sin\beta + \omega_{ib}^{pitch}\sin\alpha.\sin\beta \tag{9}$$

In the elevation plane, roll and pitch rate components get coupled to the inner gimbal through gear coupling, and geometric coupling is zero.

3.5 Modelling of Gimbal Rates, Angles & LOS Rate

With the motor actuation and different coupling torques modelled as described above, the effective load torque T_E is obtained as

$$T_E = T_A + T_G - T_F \tag{10}$$

Inertial angular rate of the gimbals ω_{icm} is obtained as

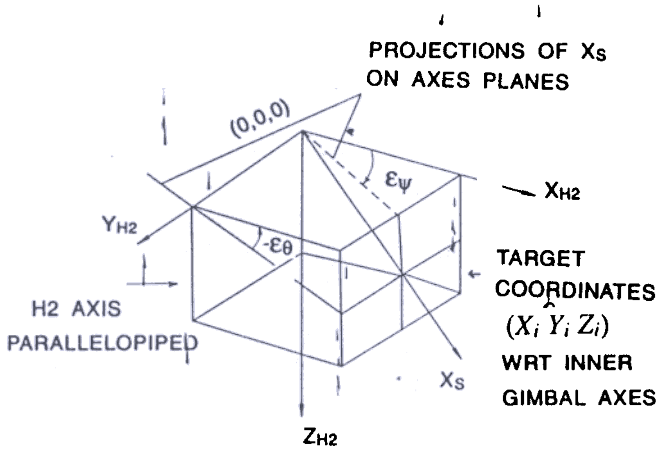

Figure 6. Definition of pointing errors

$$\omega_{icm} = \frac{1}{J} \int T_E \, dt \qquad (11)$$

Relative gimbal rate ω_{bcm} is extracted by subtracting the corresponding body rate components transformed to the gimbal system from the inertial gimbal rate ω_{icm}, i.e.

$$\omega_{bcm} = \omega_{icm} - \omega_{ib} \qquad (12)$$

where

$$\omega_{ib}^{azimuth} = \omega_{ib}^{yaw}, \quad \text{and}$$

$$\omega_{ib}^{ele} = -\omega_{ib}^{roll} \sin\alpha + \omega_{ib}^{pitch} \cos\alpha$$

This relative gimbal rate is used for back emf and friction torque modelling. The elevation gimbal angle (θ_g) and the azimuth gimbal angle (ψ_g) are obtained by integrating the corresponding relative gimbal rates, Geometrical coupling term is added to inertial gimbal rate to obtain the LOS rate as sensed by the stabilisation loop gyro for feedback (Fig. 3).

3.6 Modelling of Pointing Errors

Let the coordinate of the missile in inertial axis system be (X_M, Y_M, Z_M) and that of the target be (X_T, Y_T, Z_T). Components of the LOS vector in the inertial frame are

$$R_{XX} = (X_T - X_M)$$
$$R_{YY} = (Y_T - Y_M)$$
$$R_{ZZ} = (Z_T - Z_M).$$

Using the inertial to body rotational transformation matrix (RTM), the above components of LOS vector are transferred to the body dorsal frame. In the next step, the outer (azimuth) gimbal angle is used to get the body to outer gimbal quaternion components as per the following equation

$$e_{zob} = \cos(\psi_g/2);\ e_{1ob} = 0;\ e_{2ob} = 0;\ e_{3ob} = \sin(\psi_g/2)$$

Using this equation, the body to outer gimbal RTM is constructed and the LOS vector components are obtained in the outer gimbal axes system. Similarly, the inner (elevation) gimbal angle is used to get the outer to inner gimbal quaternion and hence the RTM. Thus, the LOS vector components are finally obtained in the inner gimbal coordinate system (X_{H2}, Y_{H2}, Z_{H2}) which are X_i, Y_i, Z_i (Fig. 6). Pointing errors sensed by the seeker are modelled in azimuth by computing the angular error between the X_{H2} axis and the projection of LOS vector X_S on X_{H2}, Y_{H2} plane and is modelled in elevation by computing the angular error between the X_{H2} axis and projection of X_S on X_{H2}, Z_{H2} plane (Fig. 6). Therefore, in terms of LOS vector components X_i, Y_i, Z_i, the pointing errors are

$$\text{Pointing error (elevation)} = -\tan^{-1}\left[\frac{Z_i}{X_i}\right]$$

$$\text{Pointing error (azimuth)} = \tan^{-1}\left[\frac{Y_i}{X_i}\right]$$

These pointing errors are the driving inputs for the seeker track loop (Fig.3).

4. APPLICATION OF 6-DOF MODEL AS DESIGN TOOL

4.1 Guidance & Control Design Validation/Tuning

For validating the guidance and control algorithm design, including its adequacy/ robustness, 6-DOF simulations incorporating different conditions are essential. First, the stability of the short period and long period dynamics is validated/established and design tuned as per requirement. Miss distance estimate is obtained next by calculating the root sum square miss of the individual miss distances due to different error sources taken one at a time in the simulation. An optimum priority-based dynamic sharing/limiting algorithm for control authority apportioning has been designed to overcome control starvation, which is more pronounced for certain zones of manoeuver plane orientations due to severe aerocross coupling effects along with CG shift. Manoeuver plane orientations ϕ (Appendix-1) would change with pitch and yaw latax. By suitably incorporating disturbances, target motions, etc. in 6-DOF, those adverse zones of manoeuver orientations have been brought out in 6-DOF simulation and the design, particularly the adequacy of the dynamic sharing/limiting algorithm established under severe aerocross coupling and CG shift disturbances.

4.2 Optimum LOS Rates for PN Mechanisation

For accurate PN guidance, latax demand is to be generated in the body frame, so that the LOS rates measured in the seeker axis (inner gimbal axis) are driven to zero, leading to a constant bearing collision course. Therefore, a novel method of obtaining optimum pitch and yaw LOS rates for PN guidance mechanisation is formulated with which the above optimum bodyframe LOS rates will result in measured LOS rates in the inner gimbal axis, when missile body to inner gimbal transformation are applied. Those optimum observed sight line rates (OBSLR) in missile body-frame are obtained (Appendix-2) as

$$\mathrm{OBSLR\,(pitch)} = \frac{\mathrm{OBSLR\,(elevation)}}{\cos(\psi_g)}$$

$$\mathrm{OBSLR\,(yaw)} = \frac{\mathrm{OBSLR\,(azimuth)}}{\cos(\theta_g)} + \mathrm{OBSLR\,(elevation)}\tan(\psi_g)\tan(\theta_g)$$

The new method of PN guidance mechanism has been validated with the help of the 6-DOF model through extensive simulation studies under different conditions and by comparing the results with those obtained by the conventional method of generating LOS rate in the bodyframe for PN guidance. With the new method, improved homing performance is achieved in terms of faster settling of errors/transients leading to lower miss distance in almost all the cases studied.

4.3 Feedforward Compensation Design

To improve the seeker isolation wrt body motion disturbances, feedforward compensation based on body-mounted autopilot gyro inputs has been designed to be given as input to the drive motor which has been modelled (Fig. 3). Since body motion coupling is partial, the amount of feedforward compensation required to be incorporated for optimum performance is obtained based on results with 6-DOF simulation model. Though feedforward compensation for azimuth/elevation channel body rate components and also for roll in elevation has shown improved performance, for azimuth channel, feedforward compensation for roll shows performance degradation in 6-DOF simulation. The reason for the above performance degradation has been brought out with the help of the simulation model. With the help of the proposed feedforward compensation for roll in azimuth channel $\omega_{ib}^{roll}\beta$, the geometrical coupling of roll rate in the seeker azimuth axis (inner gimbal Z_i axis) as derived in Section 3.4 will be effectively cancelled. However, in the process, the proposed compensation also appears in the inertial gimbal rate. Since the azimuth gimbal rotates wrt Z_o = body Z_b axis, roll rate will not get coupled to the azimuth gimbal. Thus, the above additional inertial gimbal rate developed would generate additional coupling torques through friction and back emf coupling (Fig. 3) leading to poorer performance. Based on the above studies with 6-DOF model, feedforward compensation design has been modified accordingly omitting compensation for roll in azimuth.

4.4 Switchover from Open-Loop to Closed-Loop Guidance

The 6-DOF model is used to accurately obtain the switchover point from open-loop guidance to closed-loop PN guidance, so that for different operating conditions, including subsystem errors/ biases, the required homing time is available for settling the errors/transients adequately in the presence of subsystem dynamic lags, thus ensuring the required guidance accuracy. Referring to the guided trajectory (Fig. 2), the switching from open-loop guidance (i.e. gimbal angle hold phase) to closed-loop PN guidance, has to be carried out at the specific switching sight line range r_{ss}, so that after correcting the heading error in the SPN phase (a high gain nonlinear law for navigation constant employed here where gain is reduced as the heading error is corrected), the required homing distance (or equivalently homing time) is available in the final unsaturated PN guidance phase for settling the errors/transients adequately for different operating conditions, thus ensuring the guidance accuracy. Switching with a higher sight line range compared to the optimum, r_{ss} would give lower impact angle leading to lower warhead effectiveness. The optimum switching sight line range r_{ss} is obtained from 6-DOF simulation studies with disturbances, subsystem errors, etc.

5. APPLICATION OF 6-DOF MODEL FOR PERFORMANCE EVALUATION

The 6-DOF simulation with seeker head detailed model has been extensively used for performance evaluation. Apart from an accurate estimate of terminal performance in terms of homing time/miss distance and impact angle, 6-DOF simulation with different disturbances and subsystem errors is essential to establish the adequacy of the seeker field of view and gimbal angle freedom, control deflection margins, etc. in the presence of guidance manoeuvers. Based on the 6-DOF simulation studies, the tolerance on important subsystem parameters has been so fixed that reasonable margins are available wrt the above parameters.

6. SIMULATION RESULTS & PERFORMANCE SUMMARY

The performance of the weapon system has been established for different operating conditions, including subsystem biases, errors and disturbances. Error bounds chosen are equal to the specified tolerances/error bounds of different subsystem parameters (thrust, drag and other aeroparameters, sight line rate (SLR) bias, autopilot bias, misalignment forces and moments, wind, etc.). Error sources are judiciously combined so as to bring out varying simulation conditions and performance profiles, including nominal, normal and worst case performance profiles and comparison made wrt the desired performance in terms of homing distance, impact angle, margin for gimbal angle and seeker field of view, etc. In the elevation plane, worst impact angle and homing distance condition is brought out by suitably choosing the subsystem bias errors. For example, low homing distance condition has been simulated by incorporating positive SLR and positive latax bias errors. For realising normal type disturbance condition, apart from subsystem bias errors, misalignment forces/moments and CG shift errors are also incorporated in different directions, i.e. pitch down, yaw right, etc. Again, all down-disturbance conditions are obtained from normal disturbance conditions with additional errors like thrust and drag variations simulating the lowest velocity, lower bounds on aeroparameters, etc. For simulating all up-disturbance conditions, the highest velocity condition and the upper bounds on aeroparameters are introduced. Performance obtained for some typical conditions of simulation are summarised in Table 1 for important parameters. It is observed that homing time varies between 2.7-3.4 s for normal disturbance conditions, due to the variations in subsystem bias errors giving either low homing distance or low impact angle condition. For all down-disturbance condition also, a similar variation in homing time is obtained between low homing distance and low impact angle condition. Seeker track loop is found to be the dominant lag in the missile guidance loop, having a bandwidth of 10 rad/s. Therefore, with a minimum homing time of 2.7 s, minimum normalised homing time $\omega_{nh}T$ obtained is 27, which may be just sufficient to give the required miss distance. It is known from literature[3] that for accurate settling of errors/transients, a minimum normalised homing time of 25 is required. Miss distance estimate has been subsequently obtained through exhaustive simulation studies and found to be within specified limits. For the seeker system, field of view = ± 20 mils, elevation gimbal angle freedom = –34°, 17° and azimuth gimbal angle freedom = ± 12°. Therefore, maximum pointing error in all the cases simulated (Table 1) has enough margin with respect to semi-field of view of 20 mils, whereas enough margins with respect to gimbal angles are not available for many cases. Table 1 shows impact angle, i.e., pitch attitude θ at impact to target varying between 18° and 32°, which would be improved in the near future through switching later to closed-loop PN guidance, once the seeker bandwidth and performance are improved. Typical 6-DOF performance profiles of some flight variables are shown in Figs 7-10 for nominal condition (with initial rates at tube exit). Pitch latax profile (Fig. 7) shows that latax demand from

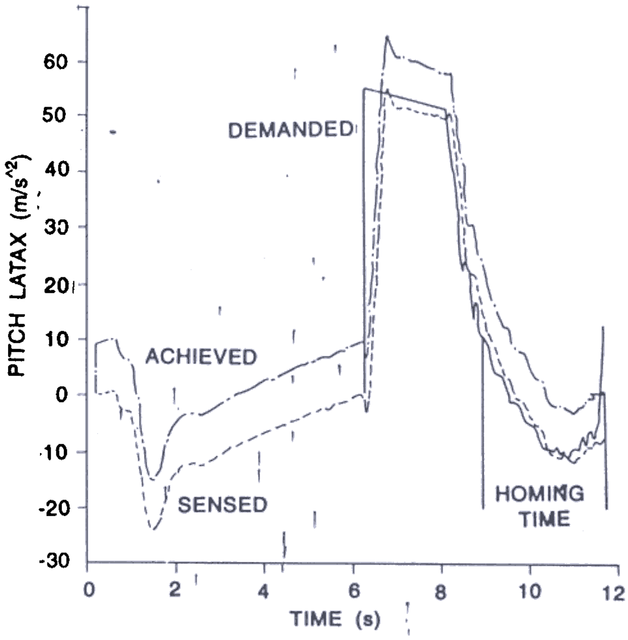

Figure 7. Nominal lateral acceleration profile (pitch)

guidance is closely followed by the autopilot. Autopilot bandwidth is validated by taking zoomed plot of demanded and sensed latax. Homing time calculated from the instant of latax demand ≤ 1 g or achieved latax ≤ 2 g (whichever occurs early) is 2.87 s (Fig. 7), giving a normalised homing time

Table 1. 6-DOF performance summary

Condition of simulation	Homing time (s) $\omega_{nh}T$(rad)	Impact angle (deg)	Maximum gimbal angle (deg) Elevation	Azimuth	Maximum pointing error (mils) Elevation	Azimuth	Maximum body rate (deg/s) Yaw	Roll	Remarks
Nominal with initial rates	02.87 28.70	-27	-30.0 09.0	-01.6	08.0	4.5	10	10	Smooth profiles, sufficient control margin
Yaw right, low homing distance, normal disturbance	02.70 27.00	-32	-30.5 09.5	08.5	09.0	8.0	38	40	Smooth profiles, reasonable control margin
Yaw right, low impact angle, normal disturbance	03.4 34.0	-20	-30.5 13.0	-08.5	10.0	7.0	40	40	Smooth profiles, reasonable control margin
Yaw right, low homing distance, all down disturbance	02.87 28.70	-30	-30.5 11.0	-10.5	09.0	6.5	43	42	Roll, yaw oscillations during full manoeuver phase
Yaw right, low impact angle, all down disturbance	03.50 35.00	-18	-30.5 15.5	10.0	10.0	6.0	44	43	Roll, yaw oscillations during full manoeuver phase

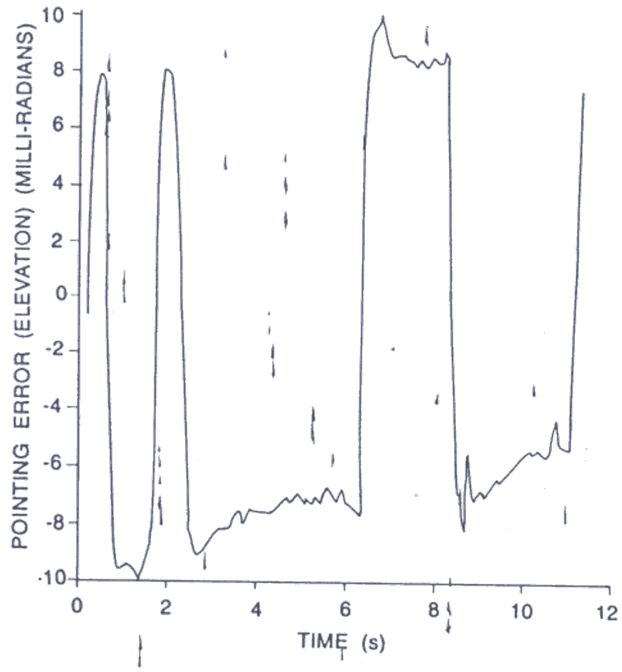

Figure 8. Nominal pointing error profile (elevation)

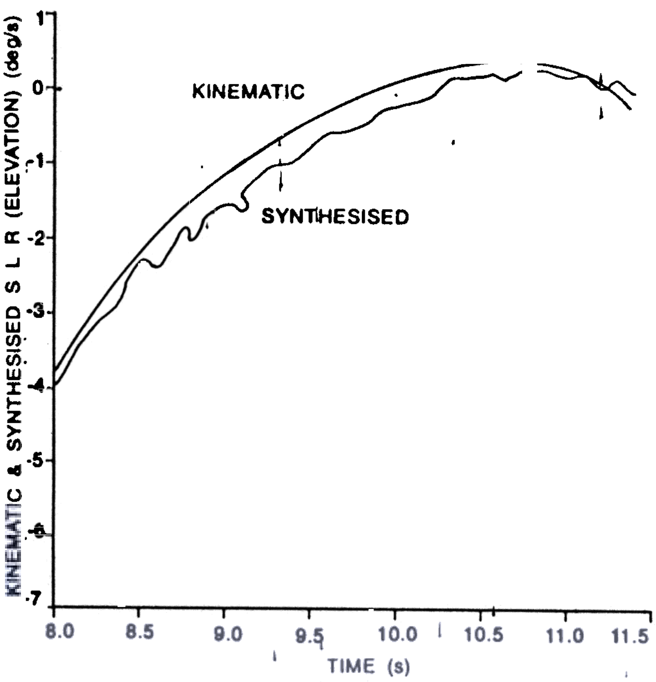

Figure 9. Nominal profile for kinematic and synthesised sight line rate (elevation).

$\omega_{nh} T = 28.7$. Since this is more than the minimum required normalised homing time of 25, the achieved latax profile shows latax staying near zero value during the last one second before

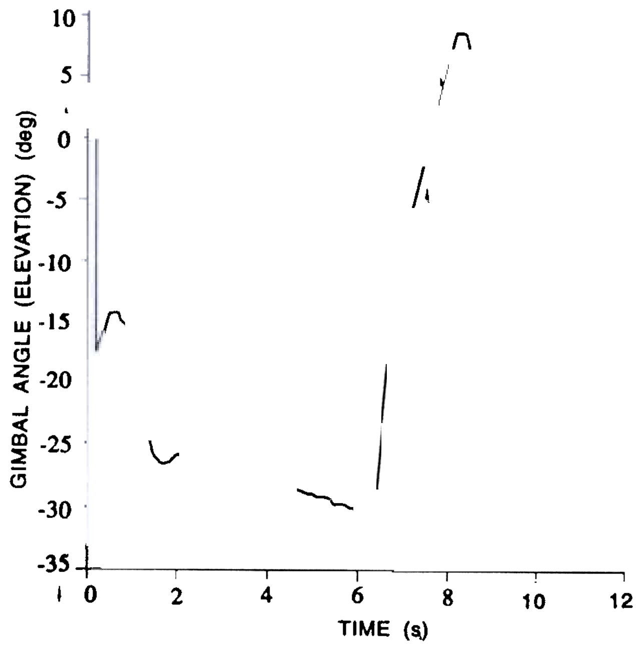

Figure 10. Nominal gimbal angle profile (elevation)

interception, signifying accurate homing to target. Pointing error profile (Fig. 8) shows that the pointing error stays within ± 10 mils, giving enough margin with respect to semi-field of view. Zoomed plot of kinematic and synthesised sight line rate signal in elevation plane, as obtained from the seeker (Fig. 9) shows that seeker- servosystem in 6-DOF is following the kinematic sight line rate with lag as per the designed bandwidth, thus validating the model. Gimbal angle (elevation) profile (Fig. 10) shows that the maximum gimbal angle goes up to 30°, giving 4° minimum margin with respect to the gimbal angle freedom.

7. CONCLUSION

The NEM for seeker-servosystem simulation has been evolved and successfully integrated in the 6-DOF model for homing missiles. In this new modelling approach, drive motor rates are considered as inertial gimbal rates and body motion coupling is modelled through forces and moments transformed to the seeker. Therefore, this model would give exact body coupling effect on the homing system, unlike the conventional velocity injection model (VIM), where full body motion is assumed coupled to the seeker system[1,2]. With exact body coupling effect modelled, the corresponding 6-DOF model integrated with NEM-based seeker system would give accurate performance projections for homing missile. Important sources of body motion coupling to the seeker head for a typical homing missile are found to be:

(a) Coupling through gears

(b) Back emf coupling

(c) Coupling through friction, and

(d) Geometrical coupling

While the components of body rates coupled to the seeker through geometric coupling depend on the gimbal angles, gear coupling and friction torque coupling to the seeker are found to be equivalent in general to the partial body motion injection.

The 6-DOF simulation model developed has been found to be a very useful design tool. For validating/tuning guidance and control algorithm design, including its adequacy/robustness, 6-DOF simulations incorporating different conditions are essential. Also, the 6-DOF model is used to accurately obtain the desired switchover point from open-loop to closed-loop PN guidance, which is required to meet the specified performance of the missile system. As the base motion coupling is found to be partial in the NEM-based modelling of the homing missile developed, the amount of feedforward compensation required for improving the seeker isolation wrt body motion disturbances can be accurately obtained based on simulation studies with 6-DOF model. A novel method of obtaining optimum pitch and yaw LOS rates for PN guidance mechanisation is formulated based on observed sight line rates measured in the seeker inner gimbal axis. The superiority of this new method *vis-a-vis* the conventional method of generating LOS rates[3] has been established through simulation studies, using the 6-DOF model developed.

8. ACKNOWLEDGEMENTS

The authors express their sincere gratitude to Prof T.K. Ghoshal, Jadavpur University, Calcutta and Shri T.V. Rao, Scientist, Research Centre Imarat, Hyderabad, for useful suggestions. They are also thankful to Mr S.V. Joshi, Scientist, Defence Research & Development Laboratory (DRDL) and Mr S.K. Dash, Consultant, DRDL for suggestions and help.

REFERENCES

1. William Nesline & Paul Zarchan. Line of sight reconstruction for faster homing guidance. *Journal of Guidance, Control and Dynamics*, 1985, 3(1), 3-8.

2. William Nesline & Paul Zarchan. Digital homing guidance—stability *vs* performance trade-offs. *Journal of Guidance, Control and Dynamics*, 1985, 8(2), 255-61.

3. Garnell, P. Guided weapon control system, Ed. 2 Pergamon Press, Oxford, 1980.

APPENDIX 1

Here, typical 6-DOF equations are presented in fin-axis frame X_f, Y_f, Z_f (Fig. A.1)

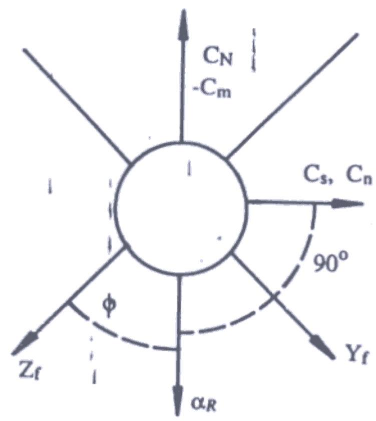

ϕ = Manoeuver plane roll orientation with respect to Z_f axis.

C_N, C_m, side force coefficient C_s, yawing moment coefficient C_n, rolling moment coefficient C_l are obtained as a function of α_R and ϕ as per aero data estimated from wind tunnel test. C_s and C_n are defined 90° anti-clockwise with respect to manoeuver plane, i.e. α_R direction.

Referring to Fig. A.1, the components of normal and side force coefficients along Z_f and Y_f axis are

$$C_{NAN} = -C_N \cos(\phi)\ ;\ C_{NAS} = -C_s \sin(\phi) \quad \text{(along } Z_f \text{ axis)}$$

$$C_{NBN} = -C_N \sin(\phi)\ ;\ C_{NBS} = C_s \cos(\phi) \quad \text{(along } Y_f \text{ axis)}$$

Pitching and yawing moment coefficients about CG, i.e. C_{mXCG} and C_{nXCG} are obtained from the corresponding aero-datas C_m and C_n given with respect to nose and thereafter, components of C_{mXCG}, C_{nXCG} along Z_f and Y_f axes are obtained as per relations given below

$$C_{mXCGA} = C_{mXCG} \cos(\phi)\ ;\ C_{nXCGA} = C_{nXCG} \sin(\phi)$$

$$C_{mXCGB} = -C_{mXCG} \sin(\phi)\ ;\ C_{nXCGB} = C_{nXCG} \cos(\phi)$$

C_{LETA} and C_{LZIE} are control force coefficients along Z_f and Y_f directions respectively, and ΔZ_f, ΔY_f are lateral CG shifts along Z_f and Y_f axes. The equations for $\dot{U}$, $\dot{v}$ and $\dot{w}$ are

$$U = rv - qw + \frac{1}{m}\left[T_X - QSC_{DO}\right] + (g_X)_f$$

$$\dot{v} = pw - rU + \frac{QS}{m}\left[C_{NBN} + C_{NBS} + C_{LZIE} + \frac{d}{2v_a}\left(-C_{Y\dot{\beta}}\dot{\beta} - C_{Y_r}r\right)\right] \frac{T_Y}{m} + (g_Y)_f + \text{terms due to misalignments}$$

$$\dot{w} = qU - pv + \frac{QS}{m}\left[C_{NAN} + C_{NAS} - C_{LETA} + \frac{d}{2v_a}(-C_{Zq}q - C_{Z\dot{\alpha}}\dot{\alpha})\right] + \frac{T_Z}{m} + (g_Z)_f + \text{terms due to misalignments}$$

Defining C_{meta} and C_{mzie} as control moment coefficients about Y_f and Z_f axis respectively, and also C_{lzeta} as roll effectiveness of control fins per pair, the equations for angular acceleration about X_f, Y_f and Z_f are.

$$p = \frac{1}{I_{XX}}\left[-I_{XX}p + T_{mX}\right] + \frac{QSd}{I_{XX}}\left[\frac{d}{2v_a}C_{lp}p - \frac{C_{lzeta}}{2}\left(eta_1+eta_3+zie_2+zie_4\right) + C_l\right] + \frac{1}{I_{XX}}(T_Y + \text{aero-forces along } Y_f).\ \Delta Z_f$$
$$- (T_Z + \text{Aero-forces along } Z_f).\ \Delta Y_f + \text{terms due to misalignments}$$

$$\dot{q} = \frac{1}{I_{YY}}\left[T_{mY} - \left(I_{XX} - I_{ZZ}\right)pr - \dot{I}_{YY}q\right] + \frac{QSd}{I_{YY}}\left[-C_{meta} + C_{mXCGA} + C_{nXCGA} + \frac{d}{2v_a}\left(C_{mq}q + C_{m\dot{\alpha}}\dot{\alpha}\right)\right] + \left[-T_X - (-QSC_{DO})\right]\frac{\Delta Z_f}{I_{YY}}$$

+ terms due to misalignments.

$$\dot{r} = \frac{1}{I_{ZZ}}\left[T_{mZ} - \left(I_{YY} - I_{XX}\right)pq - \dot{I}_{ZZ}r\right] + \frac{QSd}{I_{ZZ}}\left[-C_{mzie} + C_{nXCGB} + C_{mXCGB} + \frac{d}{2v_a}\left(C_{nr}r - C_{m\beta}\dot{\beta}\right)\right] + \left[T_X + (-QSC_{DO})\right]\frac{\Delta Y_f}{I_{ZZ}}$$

+ terms due to misalignments.

APPENDIX 2

Here, the optimum LOS rates referred to missile body frame Ω_{Ym}, Ω_{Zm} are obtained. Those optimum LOS rates are such that they would result in measured LOS rates in the inner gimbal axis Ω_{Yi}, Ω_{Zi} when missile frame to inner gimbal axes transformation $[A]_{mi}$ is applied on those optimum rates.

With $\Omega_{Xm} = 0$ as per existing guidance scheme and postulating each of Ω_{Ym}, Ω_{Zm} as a linear combination of Ω_{Yi} and Ω_{Zi}, we have

$$\begin{aligned} \Omega_{Ym} &= a\,\Omega_{Yi} + b\,\Omega_{Zi} \\ \Omega_{Zm} &= c\,\Omega_{Yi} + d\,\Omega_{Zi} \end{aligned} \qquad \text{(B.1)}$$

Noting that the outer gimbal moves with respect to body Z_m axis by azimuth gimbal angle α and the inner gimbal moves with respect to the outer gimbal Y_o axis through elevation gimbal angle β (Fig. 5), the missile frame to inner gimbal axis X_i, Y_i, Z_i rotational transformation matrix $[A]_{mi}$ is obtained as

$$[A]_{mi} = \begin{bmatrix} \cos\alpha\cos\beta & -\sin\alpha\cos\beta & -\sin\beta \\ \sin\alpha & \cos\alpha & 0 \\ \sin\beta\cos\alpha & -\sin\alpha\sin\beta & \cos\beta \end{bmatrix} \qquad \text{(B.2)}$$

From Eqns (B.1) and (B.2), the definition of optimum LOS rates, as suggested above, gives

$$\begin{bmatrix} \Omega_{Xi} \\ \Omega_{Yi} \\ \Omega_{Zi} \end{bmatrix} = \begin{bmatrix} \cos\alpha\cos\beta & -\sin\alpha\cos\beta & -\sin\beta \\ \sin\alpha & \cos\alpha & 0 \\ \sin\beta\cos\alpha & -\sin\alpha\sin\beta & \cos\beta \end{bmatrix} \begin{bmatrix} 0 \\ a\Omega_{Yi} + b\Omega_{Zi} \\ c\Omega_{Yi} + d\Omega_{Zi} \end{bmatrix}$$

The following equations are obtained

$$\Omega_{Yi} = a\cos\alpha\,\Omega_{Yi} + b\cos\alpha\,\Omega_{Zi}$$

$$\Omega_{Zi} = -a\sin\alpha\sin\beta\,\Omega_{Yi} - b\sin\alpha\sin\beta\,\Omega_{Zi} + c\cos\beta\,\Omega_{Yi} + d\cos\beta\,\Omega_{Zi}$$

Eqns (B.4) and (B.5) are solved to obtain

$$a = \frac{1}{\cos\alpha} \quad b = 0, \; c = \tan\alpha\tan\beta \text{ and } d = \frac{1}{\cos\beta}$$

From Eqn (B.1), the optimum LOS rates referred to missile body coordinates are

$$\Omega_{Ym} = \left(\frac{1}{\cos\alpha}\right)\Omega_{Yi}$$

$$\Omega_{Zm} = \tan\alpha \tan\beta \, \Omega_{Yi} + \left(\frac{1}{\cos\beta}\right)\Omega_{Zi} \qquad \text{(B.6)}$$

Contributors

Shri RN Bhattacherjee obtained his BE (Electrical Engineering) from Jadavpur University, Calcutta in 1970 and MTech (Guidance and Control) from Indian Institute of Technology, Madras, in 1976. He joined DRDO in 1977, as Scientist, at DRDL. The areas of his research include guided missile systems, covering system design, specifications, guidance and control algorithms, modelling, simulation and performance evaluation. Presently, he is working on design, modelling and simulation for a third generation antitank missile.

Shri A Saha obtained his BTech (Electrical Engineering) from Calicut University, Kerala, in 1988 and ME (Control & Guidance) from Jadavpur University, Calcutta, in 1992. He joined DRDO as Scientist at the Defence Research & Development Laboratory (DRDL), Hyderabad, in 1992. Presently, he is working on design, modelling and digital simulation of control and guidance systems for a third generation antitank missile. He is a life member of the Astronautical Society of India.